Paper No.
08396

NACE INTERNATIONAL CORROSION 2008 CONFERENCE & EXPO

Corrosion Assessment of Mechanically Formed Aluminized Steel

Mersedeh Akhoondan, Alberto A. Sagüés
Department of Civil and Environmental Engineering, University of South Florida, 4202 East Fowler Ave., Tampa, FL 33620, U.S.A.

Leonardo J. Cáseres
Mechanical & Materials Engineering Division Southwest Research Institute 6220 Culebra Road San Antonio, Texas 78238-5166

ABSTRACT

Ribbed steel pipes made of Type 2 aluminized steel are commonly used for culverts, which are required to have long service life. However, early corrosion of aluminized steel pipes has been recently observed in some inland locations. Fabrication of sharp bends might cause aluminized coating fissures leading to early corrosion. The extent of brittle failure of the inner, intermetallic aluminized layer as function of simple bending radius was quantified. Electrochemical impedance spectroscopy was used to measure corrosion rate of both formed and flat aluminized steel samples in simulated natural waters. Initial findings show that specimens formed by spherical indentation were susceptible to early corrosion development in moderately aggressive simulated natural water, but less so in a more benign, precipitating simulated natural water solution.

Key Words: Corrugated, Microfissures, Scale-forming waters, Bent metal sheets, Corrosion

INTRODUCTION

Aluminized steel Type 2 is produced as a steel sheet hot dip coated on both sides with commercially pure aluminum (ASTM A929 and ASSHTO M274), which provides corrosion protection through low corrosion rate of the aluminum when the aluminum is in passive condition, and also may confer galvanic protection to the exposed underlying steel under certain circumstances[1]. For that reason, aluminized steel Type 2 is increasingly used for metallic drainage components in contact with natural waters. However, corrosion is an important durability limitation factor in these components which are often designed for very long service life (e.g. 75 yr) [2].

Microscopic examination of aluminized steel Type 2 in cross section shows a nearly pearlite-free ferrite low carbon steel substrate with regular grains, a partly columnar brittle inner alloy layer ~15 μm thick, and a softer outer aluminum-rich layer ~30 μm thick. The inner alloy layer, commonly of composition Fe_2Al_5 [3, 4] is an essential ingredient of the coating protection system, supplementing the outer aluminum-rich layer and possibly providing a second line of defense against corrosion. The composition of the outer layer is predominantly nearly pure aluminum with Fe-rich intermetallic precipitates (6-11 wt% Fe) [5]. During manufacturing and/or handling of the final material, discontinuities in the aluminized coating can extend to the substrate steel, creating coating breaks. Those coating breaks exposing the steel base may result in the formation of galvanic macrocells. However, if the environment is mild as those commonly found in Florida inland waters, sacrificial protection to the exposed underlying steel may not be sufficient to prevent early corrosion.

Ongoing field inspections, conducted by Florida D.O.T. on spiral rib aluminized steel Type 2 culvert pipes exposed to Florida inland waters for only a few years, have shown severe corrosion damage in the form of pits and generalized corrosion at the pipe ribs (where extended material bending occurred), but less so at the flat portions of the pipe. The possible causes of the deterioration are under investigation, which includes the present study.

This work aims at determining the corrosion behavior of mechanically formed aluminized steel Type 2. The microstructural aspects of mechanical distress upon bending as a precursor to corrosion development are characterized. Specimens with various bending radii of curvature are electrochemically assessed in waters of varying scaling tendencies with moderate chloride content, resembling compositions typically found in inland Florida waters. The investigation is in progress and initial findings are presented here, to be amplified in the future as additional information is developed.

EXPERIMENTAL PROCEDURE

Microstructural assessment of mechanical distress due to bending has been performed to date with 16-gage (1.58 mm thick) Type 2 aluminized steel sheets simply bent to various extents. The bent region was mounted metallographically. The cross section of the outer bent was examined at low magnification and digitized to determine local radius of curvature. The same regions were then examined at high magnification to determine the type and extent of distress. Future tests will address the deformation of samples formed by spherical indentation as those described in the next paragraph.

Circular 16-gage aluminized steel specimens with exposed area of 12.6 in^2 (82 cm^2), and with minimal as-received surface distress were indented at the center to a hemisphere shape using stainless steel ball-bearing balls with diameters of 1 in (2.54 cm) , 3/4 in (1.90 cm), and 9/16 in (1.43 cm) (Figure 2). The indentation was made by pressing the bearing ball, socketed in a steel plate into the initially flat specimen. An indented Teflon plate was used to protect the convex face of sample until full hemispheric penetration was achieved. The convex face was the one later exposed to the test solution. After forming the specimens were cleaned with ethanol and acetone, and stored in a desiccator prior to immersion. Figure 3 shows the appearance of the dimpled specimens. Control flat specimens without surface indentation were also used for comparison. Multiple specimens were prepared for duplicate testing.

A three-electrode test cell (Figure 4) was designed for exposing horizontally the convex side of the specimen, where distress is expected to be worst because of the tensile stresses. Corrosion of the concave side will be assessed in future experiments. A metal-metal oxide activated titanium mesh placed parallel ~6 cm from the specimen surface was used as a counter electrode, while a low impedance activated titanium pseudo reference electrode 0.3 cm diameter and 5 cm long was placed ~1.5 cm above the specimens' indentation and periodically calibrated against a saturated calomel reference electrode (SCE). All potentials reported here are in the SCE scale. Each test cell was filled with 500 mL of a solution, not replenished during the test as explained below.

Two test solutions (Table 1) were prepared from de-carbonated de-ionized water of resistivity>10^6 Ω-cm combining reagent grade NaCl and NaOH (solution C of negligible carbonate precipitating tendency) and $NaHCO_3$, HCl, and $Ca(OH)_2$ (solution P of high carbonate precipitating tendency). The Langelier Index was -5.9 for solution C and +1.50 for solution P, consistent with the observation of a ~0.5 mm thick powdery precipitate layer of $CaCO_3$ uniformly distributed on the specimen surface shortly after initiation of exposure. The test solutions in the test cells were quiescent and naturally aerated through a small opening. The relatively small electrolyte volume/total specimen area ratio was intended to be representative of, for instance, worst-case culvert pipe conditions with stagnant water on the pipe invert, or of occluded conditions for pore water on the soil side of a pipe.

The immersion tests were conducted in duplicate at 22±2˚C. Solution pH, conductivity, and open circuit potential (E_{OC}) were monitored periodically. Electrochemical impedance spectroscopy (EIS) measurements were obtained at the E_{OC} with a Gamry™ PCI4-300 potentiostat in the frequency range from 100 kHz to 1 mHz using sinusoidal signals of 10 mV rms amplitude. The tests are in progress and results for the ~1,000 hours initial period are presented here.

RESULTS AND DISCUSSION

Metallographic Analysis

Figure 1 (left) shows a metallographic cross section of the as-received (flat) material showing the coating microstructure described in the Introduction. Figure 1 (right) shows the coating condition of a bent sample (radius ~2 mm). The most notable feature is nearly completely brittle fracture of the intermetallic layer, as manifested by its many elongation gaps. The outer coating was much more ductile, with few instances of fracture as that illustrated on the left side of the right figure, apparently originating at one of the larger brittle gaps of the inner layer. The number and severity of fractures in the inner layer increased as the bending stress increased. For completely brittle fracture, the integrated gap length measured on a line parallel to the perimeter, divided by the initial length (that is, that of the remaining visible intermetallic) should equal the total strain at the outer fiber. To test that hypothesis, the strain ε_M calculated from measurements of the ratio of inner layer gaps to visible intermetallic length was compared with the strain at the outer fiber expected from the local macroscopic bending radius and the sheet thickness. For a simply bent sheet in which the neutral axis of metal sheet stays constant, the theoretical relationship between the strain of outer fiber and radius of curvature [6] is:

$$\varepsilon_I = \frac{T}{2\left(R - \frac{T}{2}\right)} \qquad \text{Eq(1)}$$

where:
ε_I is the ideal strain
T is the thickness of the sheet (16-gage = 1.58 mm)
R is the outer bending radius

Figure 5 compares the values of ideal outer fiber strain computed per Eq. (1) from the radius of curvature determined for various specimens from the low magnification micrographs and the sheet thickness, and ε_M from the micrographic analysis of the intermetallic layer. Flat samples were assigned a radius > 50 mm in the graph. The results support the hypothesis of nearly completely brittle behavior for the inner intermetallic layer. Tests in progress address behavior of specimens bent by spherical indenting and ductile fracture of the outer layer, which will be reported in the future.

Direct observation of corrosion performance

Visual examination of the specimen surfaces in solution P (high total alkalinity with carbonate precipitation) showed early appearance of light yellowish discoloration uniformly distributed over the convex indentation surface in all dimpled specimens tested, indicative of ongoing corrosion there (Figure 6). Symptoms were more sever in solution C (low alkalinity and no precipitating tendency), where appearance of strong reddish discoloration was first noted early on in the exposure around the convex indentation of all dimpled specimens, and gradually propagating covering the entire indentation surface (Figure 7). Corrosion appeared to be more intense for the 1-in diameter indentation specimens, although it is noted that the affected area was greatest for those even though maximum local strain may have been less severe than for the smaller radius indentation specimens. In both solutions, corrosion of the surrounding aluminized surface was minimal, suggesting preservation of passive behavior there during the test interval sampled. Correspondingly, no sign of corrosion was observed in any of the flat surface specimens exposed to both solutions, suggesting good corrosion performance to date in those cases. Clearly, for the time being any galvanic protection from the aluminized portion was insufficient to avoid initiation of active corrosion of the exposed steel especially in the C solution, in agreement with the results reported elsewhere for specimens with machined coating breaks [7].

EIS measurements

EIS results are exemplified for two typical cases in Figure 8. In one set of cases, usually early during the test exposure, the impedance behavior could be accurately fit to that of an analog circuit consisting of a solution resistance in series with a parallel combination of a non-ideal capacitor and a resistor. In the rest of the cases the impedance diagrams showed two time constants and the impedance behavior could be closely approached by incorporating an additional resistor-capacitor parallel combination in series. After subtracting the solution resistance, the value of the resistance of the single resistor or the sum of the two resistors respectively was designated as the apparent polarization resistance Rp of the system and used as an inverse descriptor of the effective corrosion current. Figure 9 shows the resulting values of Rp of duplicate specimens in the C and P solutions, at various exposure times and for the various dimple radii used.

The Rp values were typically much greater in the P solution, in agreement with the expected more benign character of that precipitating solution. Rp there tended to increase with time, indicating a maturing of the protective regime. Furthermore, there was little differentiation between the Rp values of the flat and dimpled specimens, indicating that the light corrosion manifested by direct observation had likely been arrested in this medium after some initial active period. These results are consistent with protective regimes reported by Caseres[8] for blemished aluminized steel in the same solution.

The Rp values correspond to more aggressive conditions in the C solution, in agreement with visual observations. There the Rp values were generally much lower than in P, and decreased with time indicating increasing corrosion. Moreover, Rp in the dimpled specimens was generally lower than in the flat specimens, indicating an adverse effect of forming. It is noted however that one of the duplicate flat specimens experienced a significant decrease in Rp before 46 days of exposure, which may be indicative of onset of protective corrosion by the aluminized layer[1,7] but also possible development of crevice corrosion artifacts in the cell. Continuing test with multiple replicates is being implemented to elucidate this issue.

At this time, no clear differentiation in behavior has been established between specimens formed with different radii indentations, in part because of the early stage of the tests and also because the relative area of the mechanically distressed zones has not been quantitatively determined. Long-term monitoring of specimens, and development of ways to account for surface area normalization of corrosion at the different indentation sizes, is in progress.

CONCLUSIONS

1. Forming by bending results in brittle fracture of the inner (intermetallic) aluminized coating layer, in a manner consistent with predictions of simplified bending mechanics of the system. Failure of the outer (mostly aluminum) layer by ductile deformation was much less common.

2. The convex portion of specimens formed by spherical indentation was susceptible to early corrosion development in moderately aggressive simulated natural water. Not formed (flat) aluminized control surfaces showed much less deterioration during the test interval (from visual and electrochemical evidence).

3. Both formed and control specimens showed little corrosion damage when exposed to a more benign, precipitating simulated natural water solution.

4. Impedance spectroscopy measurements were generally in agreement with the visual observation trends.

5. The above are preliminary findings from tests in progress. Confirmation as well as revealing the evolution of other modes of deterioration is pending on longer term evaluation with the test assemblies created in the present work. .

6. Additional future work will focus on analyzing the strain of deep drawn specimens, and establishing a relationship between the strain and corrosion rate of exposed specimen.

ACKNOWLEDGEMENTS

This investigation was supported by the State of Florida Department of Transportation and the U.S. Department of Transportation. The opinions, findings and conclusions expressed in this publication are those of the authors and not necessarily those of the supporting agencies.

REFERENCES

1. Kimoto H. (1999), Corrosion Engineering 48, p. 579.

2. Cerlanek W.D., Powers R.G. (1993), Drainage Culvert Service Life Performance and Estimation, State of Florida Department of Transportation Report No. 93-4A.

3. An J., Liu Y.B., Sun D.R. (2001), Mechanism of Bonding of Al–Pb Alloy Strip and Hot Dip Aluminised Steel Sheet by Hot Rolling, Materials Science Technology 17, pp. 451-454.

4. Li W., Liu S., Huang Q., Gu M. (2003), Hot Dipped Aluminising (HDA) of a Low Carbon Steel Wire, Materials Science and Technology 19, pp. 1025-1028.

5. Caseres L., Sagues A.A. (2005), Corrosion of Aluminized Steel in Scale Forming Waters, Paper No. 05348, 13 pp. Corrosion/2005, NACE International, Houston, 2005.

6. Dieter G., (1986), Mechanical Metallurgy, McGraw-Hill, New York, pp 659-662

7. Cáseres and A.A. Sagüés (2006), Galvanic Behavior of Type 2 Aluminized Steel in Simulated Natural Waters", L. Cancun, Mexico, "Corrosion of Infrastructure", The Electrochemical Society, Pennington, NJ, 2007, ECS Transactions Vol. 13, Issue 13, 210th ECS Meeting , October 29-November 3, 2006, pp. 147-157

8. Caseres L. (2007), Electrochemical Behavior of Aluminized Steel Type 2 in Scale-Forming Waters, Ph.D. Dissertation, University of South Florida

9. Armstrong R.D., Braham V.J. (1996), the Mechanism of Aluminum Corrosion in Alkaline Solutions, Corrosion Science 38, pp. 1463-1471.

10. Bednar L. (1989), Galvanized Steel Drainage Pipe Durability Estimation with a Modified California Chart, Paper No. 88-0341, 68th Annual meeting, Transportation Research board, Washington, D.C.

11. Castro P., Sagues A.A., Moreno E.I., Maldonado L., Genesca J. (1996),Characterization of Activated Titanium Solid Reference Electrodes for Corrosion Testing of Steel in Concrete, Corrosion 52, p. 609.

12. AK Steel, Aluminized Steel Type 2 Product Features, (2007) http://www.aksteel.com/pdf/markets_products/carbon/T2_Data_Bulletin.pdf

13. Legault R.A., Pearson V.P. (1978), Kinetics of the Atmospheric Corrosion of Aluminized Steel, Corrosion 34, pp. 344-348.

14. Creus J., Mazille H., Idrissi H. (2000), Porosity Evaluation of Protective Coatings Electrodeposited on Steel, Surface and Coatings Technology 130, pp. 224-232.

Table 1- Solution Compositon and Properties

Solution	TA	TH	FC	BI	pH	Ca^{+2} mg/L	Cl^{-} mg/L
C (Control)	6	2	0	8	~7.4	0	372
P (Precipitating)	184	52	13	223	~7.4	200	
Preparation (Per 1 L of Solution)							
C	0.05 mL of 0.01 M Na(OH)						
	5.25 mL of 2 M NaCl						
P	100 mL of 0.1 M $NaHCO_3$						
	0.37 g of $Ca(OH)_2$						
	105 mL of 0.1 M HCl						

Legend: TA: Total Alkalinity (mg/L) of $CaCO_3$, TH: Total Hardness (mg/L) of $CaCO_3$, FC: free CO_2, α: Solution Conductivity

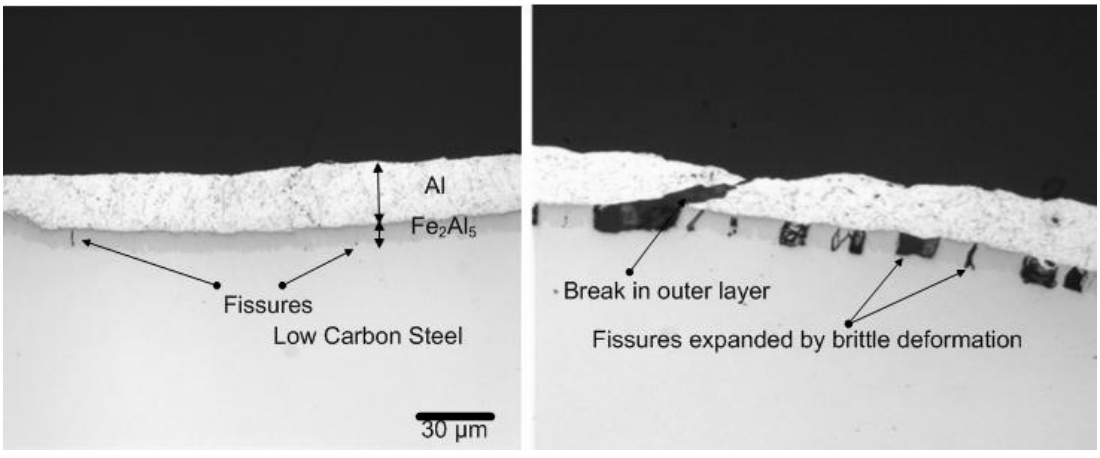

FIGURE 1 – Flat Specimen (left), Bent Specimen (right)

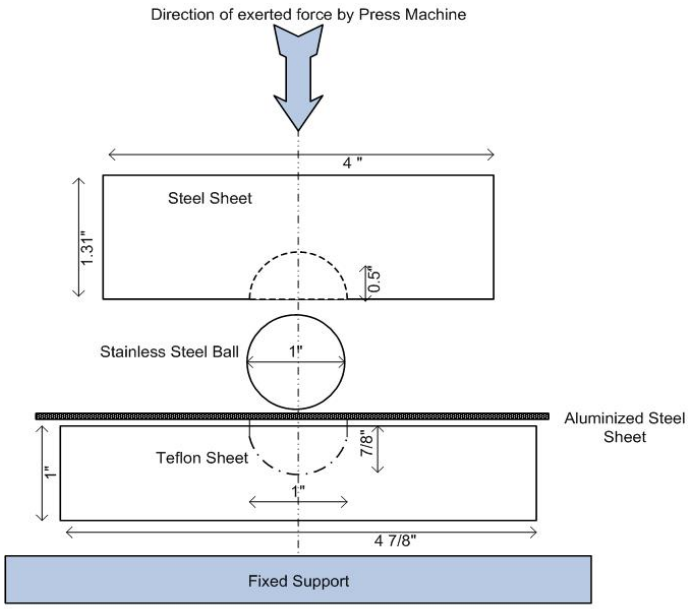

FIGURE 2 – Indentation Process

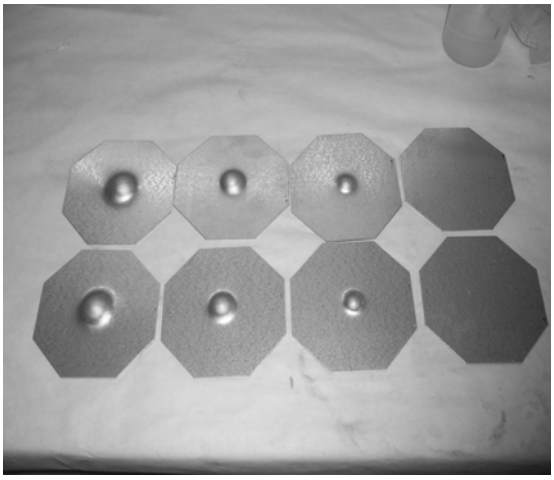

Figure 3 - Duplicate Speciments Indented to (Left to Right) 1-in, ¾-in, 9/16-in, and Flat

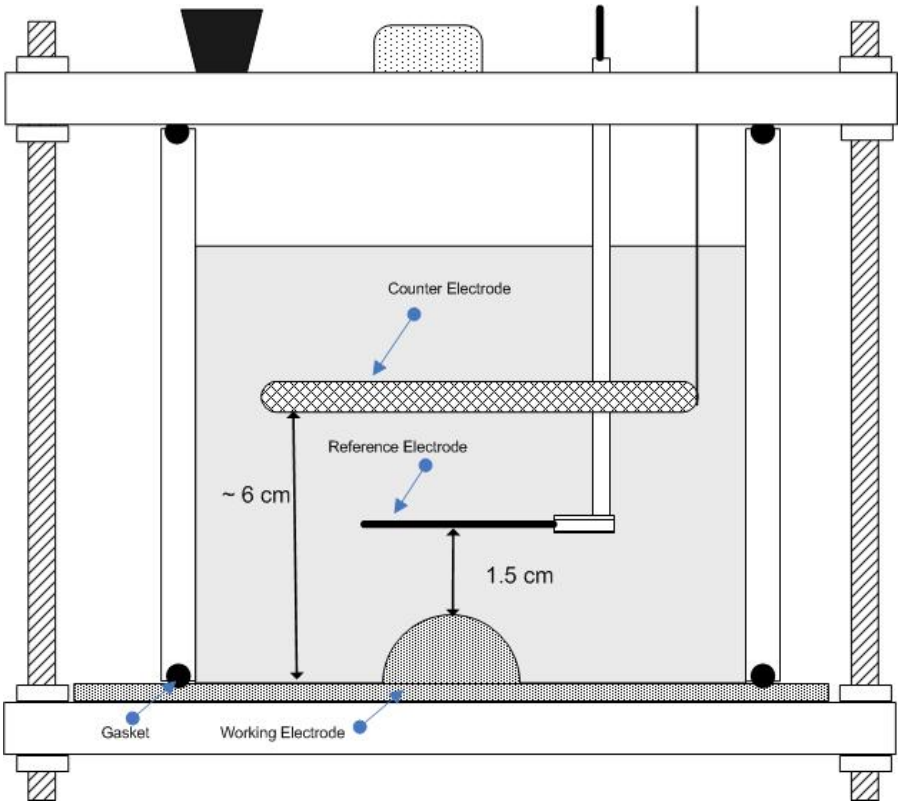

FIGURE 4 – Three-Electrode Cell Configuration

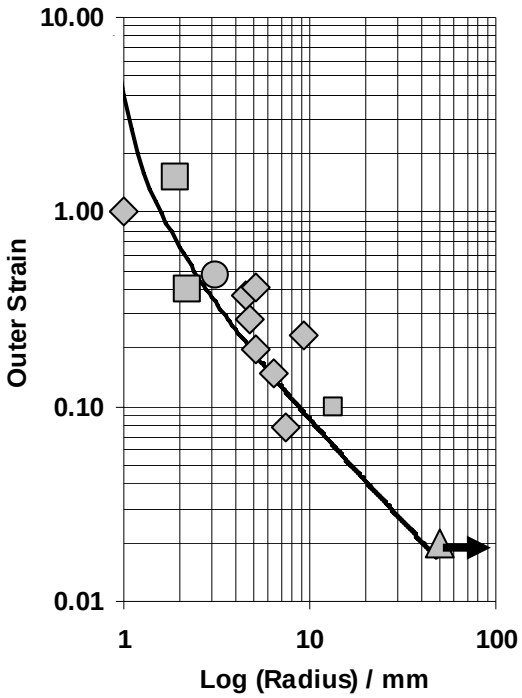

FIGURE 5 – Outer Strain ε_I per Eq(1) (solid line) and ε_M per Micrographic Analysis of Intermetallic Layer Gaps (symbols) as Function of Radius of Curvature for Various Specimens. Multiple Symbols Indicate Various Radii Locations in a Given Specimen.

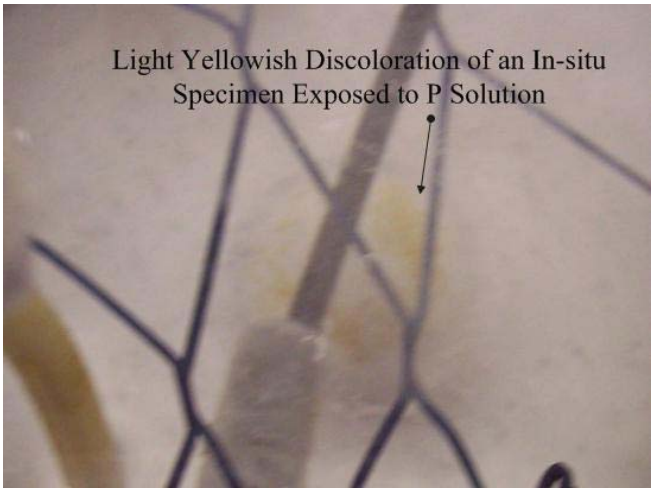

Figure 6 - Light Corrosion at a 1-in Convex Dimple Exposed to Solution P. (Picture shows immersed sample surface at 21 days exposure).

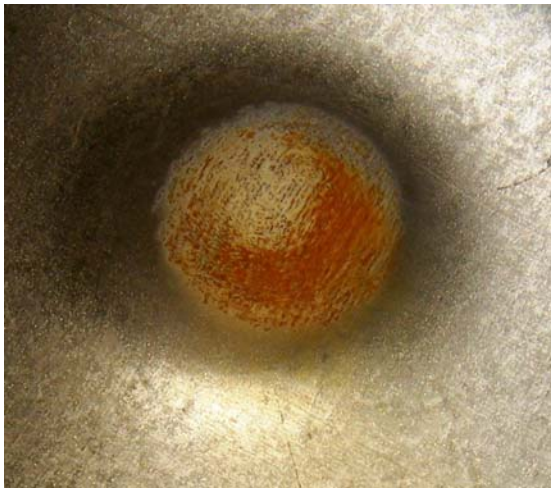

FIGURE 7 – Severe Corrosion at a 1-in Convex Dimple Exposed to C Solution (Immersed sample at age of 19 days).

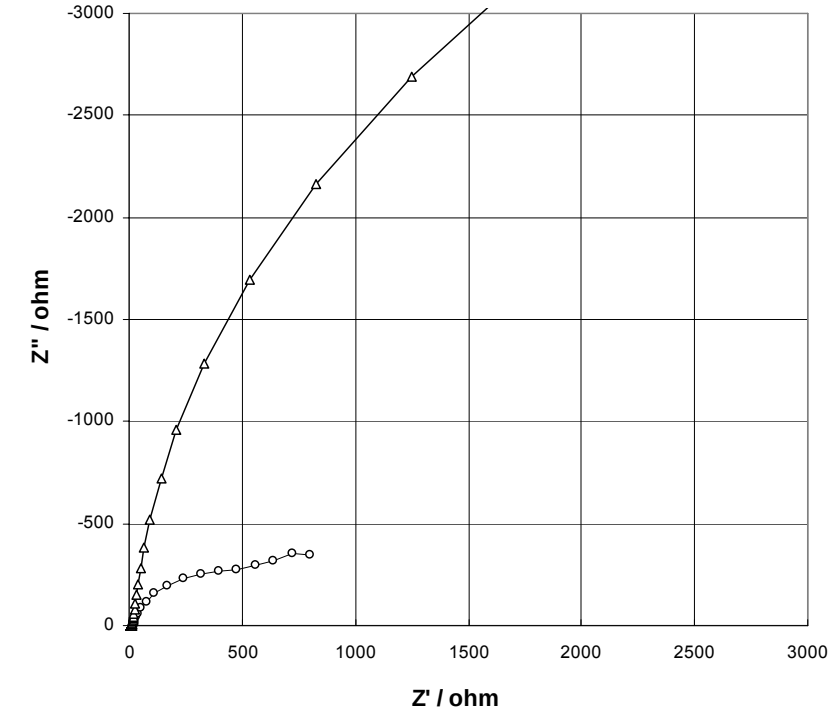

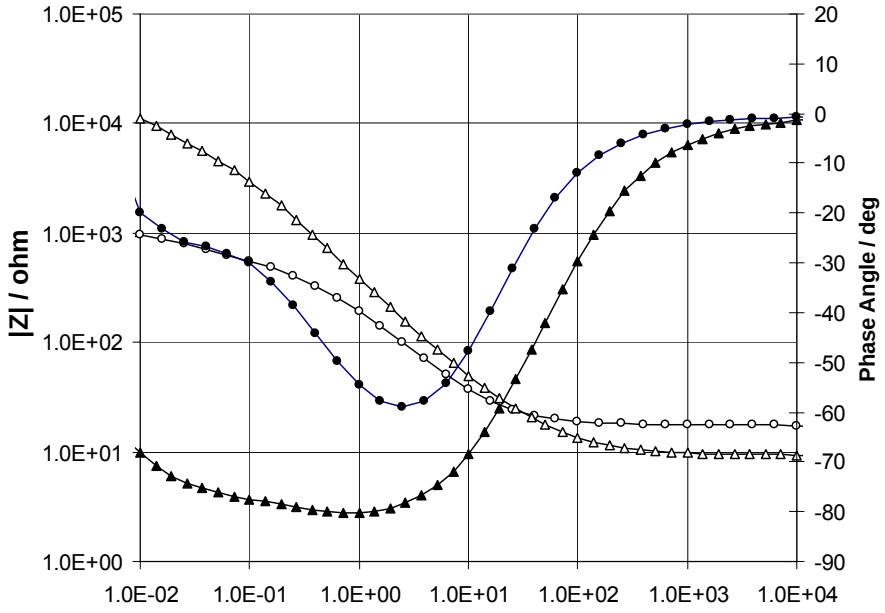

Figure 8 – Examples of EIS Results. Triangles: Flat Specimen 2, 10 days, Solution C. Circles: 1-in Indentation Specimen 1, 46 Days, Solution C.

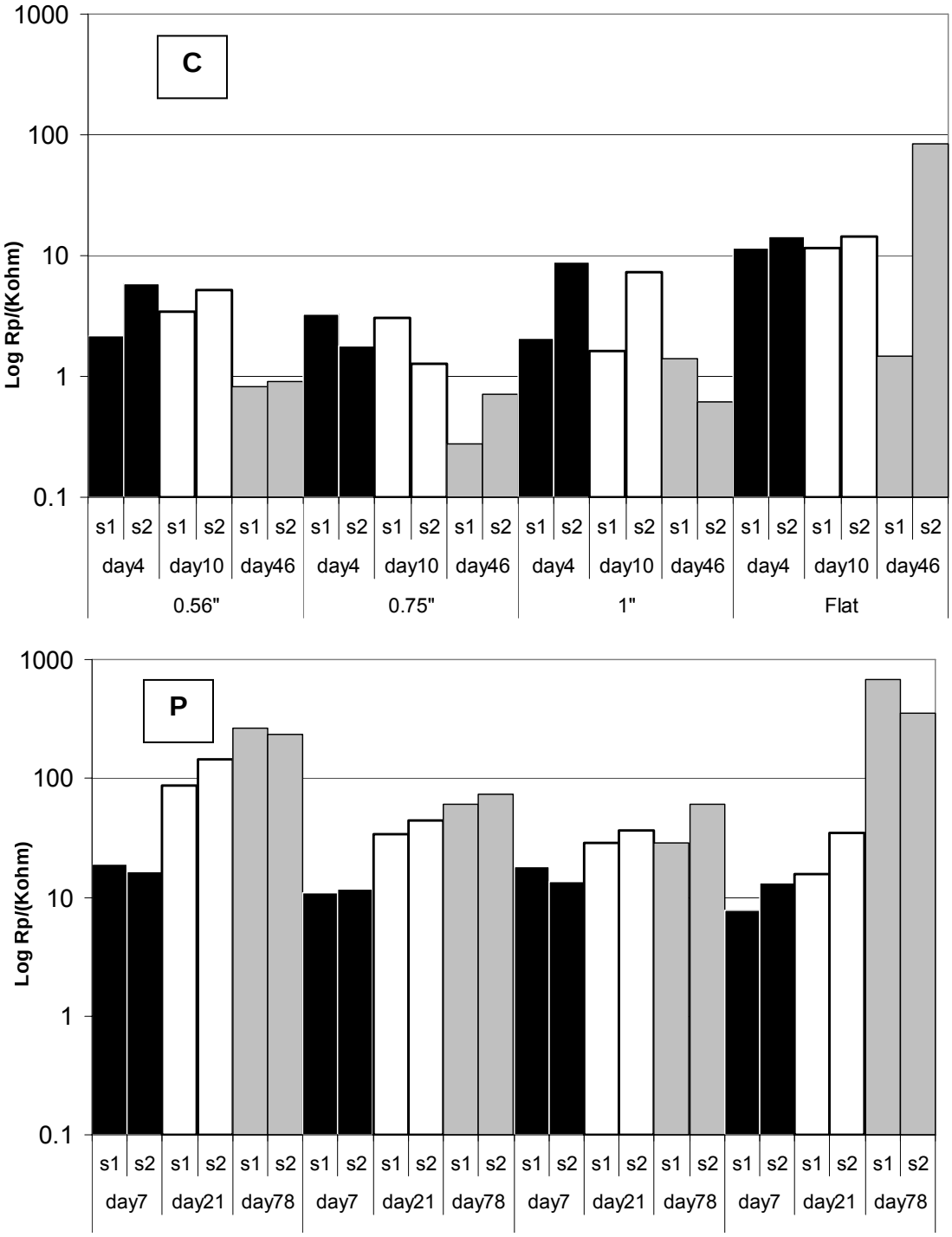

FIGURE 9 – Polarization Resistance Values for Different Bent Categories at Three Exposure Times in C Solution and in P solution (B)